Realization of high performance silicon nanowire based solar cells with large size

Realization of high performance silicon nanowire based solar cells with large size

X X Lin[1,2]**, X Hua**[1]**, Z G Huang**[1] **and W Z Shen**[1]

[1] Laboratory of Condensed Matter Spectroscopy and Opto-Electronic Physics, and Key Laboratory of Artificial Structures and Quantum Control (Ministry of Education), Department of Physics, and Institute of Solar Energy, Shanghai Jiao Tong University, Shanghai 200240, People's Republic of China
[2] Department of Mathematics and Physics, Shanghai Dian Ji University, Shanghai 201306, People's Republic of China

E-mail: wzshen@sjtu.edu.cn

Abstract

We report the realization of high performance silicon nanowire (SiNW) based solar cells with a conversion efficiency of 17.11% and a large size of 125×125 mm^2. The key factor for success lies in an efficient approach of dielectric passivation to greatly enhance the electrical properties while keeping the advantage of excellent light trapping of the SiNW structure. The suppression of carrier recombination has been demonstrated through the combination of the SiO_2/SiN_x stack, which exhibits a good passivation effect on heavily doped SiNWs via reducing both the Shockley–Read–Hall recombination and near surface Auger recombination. We have examined in detail the effects of different passivations and SiNW lengths on the effective minority carrier lifetime, reflectance and carrier recombination characteristics, as well as cell performance. The proposed passivation techniques can be easily adapted to conventional industrial manufacturing processes, providing a potential prospect of SiNW based solar cells in mass production.

(Some figures may appear in colour only in the online journal)

1. Introduction

Minimizing both optical and electrical losses are two major concerns in designing high efficiency solar cells. The enhancement of optical absorption usually focuses on anti-reflection and efficient light trapping of the incident light, while the electrical improvement concentrates on decreasing recombination rate throughout the device. Recently, the nanostructure of silicon nanowires (SiNWs) has attracted great attention, because of its excellent anti-reflection and light trapping effect [1–3], which make this structure a promising candidate to lower both the required quality and quantity of silicon material [4]. Many groups have investigated SiNW based solar cells, providing valuable support for further improvement [5–16]. However, the efficiency of SiNW based solar cells still falls behind that of the conventional crystalline silicon cells, resulting from the limitation of the extreme high surface recombination in SiNWs. The electrical properties degrade for the

accelerated recombination of photogenerated carriers, which even counteracts the benefits of optical enhancement [14]. The suppression of carrier recombination in SiNWs turns out to be the primary focus for the performance improvement of SiNW based solar cells.

Surface passivations such as thermal oxidation, carbon thin films, and chlorine dielectric treatment have been widely studied to improve the electrical characteristics of SiNW based solar cells [9, 17, 18]. Thermally grown SiO_2 is one of the most popular surface passivation techniques to reduce the Si–SiO_2 interface state density, and has been proved quite effective in the world-record solar cell [19]. Carbon thin film passivation can prolong the minority carrier lifetime of SiNWs from 10 to 21 μs [17], while the chlorine treatment presents a decrease of leakage current by five orders of magnitude [18]. It should be noted that these passivations can only work on recombination at the SiNW surface; however, a recent attempt has demonstrated that, in addition to the surface recombination, high Auger recombination near the surface

1

plays a key role in the limitation of the photogenerated carrier collection and cell efficiency in SiNW based solar cells [20]. The Auger recombination comes from the high doping related to in-diffusion through the large surface area of the silicon nanostructure. This near surface Auger recombination grows dominantly over the surface recombination, especially for the excessive doping condition in SiNW based solar cells.

In order to reduce recombination both at and near the surface in SiNWs while maintain good light trapping, we propose here an efficient method of SiN_x passivation, which has been widely employed in industrial manufacture. It is well known that SiN_x can provide not only effective surface passivation, but also bulk passivation because of the hydrogen diffusion, which effectively reduces defect state density and suppresses the Auger recombination at and near the surface [21, 22]. Another advantage of the SiN_x passivation is that we can easily adapt it to the present industrial manufacturing processes, making high efficiency SiNW based solar cells with large size possible. We have further combined this with the SiO_2 surface passivation to obtain the best recombination suppression both at and near the surface. The SiO_2/SiN_x stack performs better due to the more homogeneous $Si–SiO_2$ self-oxidation interface as well as further decreased surface state density [16, 21]. Through deep investigation of the effects of different passivations and SiNW lengths as well as effective control of carrier recombination, we have achieved a record efficiency of 17.11% on large area (125×125 mm^2) SiNW based solar cells by conventional industrial manufacturing processes. The present work opens a potential prospect for the practical fabrication of large size SiNW based solar cells with satisfactory conversion efficiency.

2. Experimental details

Figure 1 shows schematic process diagrams for the fabrication of SiNW based solar cells with different passivations. SiNWs were synthesized on one side of p-type (~2 Ω cm, B doped, 200 ± 20 μm) silicon (100) wafers with a large area of 125×125 mm^2 using a two step metal-assisted chemical etching technique [23]. The wafers were first cleaned under a standard RCA process and textured with alkaline solution. In order to have a thick silver film only on one side of each wafer, we wrapped two textured wafers together and then immersed them in a mixture of 5 mol l^{-1} aqueous hydrofluoric acid (HF) and 0.02 mol l^{-1} silver nitrate (AgNO$_3$) solution for 90 s. The length of SiNWs was based on different etching times in an aqueous buffered 5 mol l^{-1} HF and 0.01 mol l^{-1} hydrogen peroxide (H$_2$O$_2$) at room temperature. These wafers were finally dipped into nitric acid (HNO$_3$) aqueous solution to remove the capped silver and rinsed with deionized water several times.

For solar cell fabrication, all the wafers were subjected to phosphorus diffusion using oxychloride (POCl$_3$) as the dopant source at 850 °C to form a p–n junction, resulting in a sheet resistance of around 75 Ω/sq. We have divided the wafers into four series according to different passivation methods (as shown in figure 1): series A (bare SiNWs without any
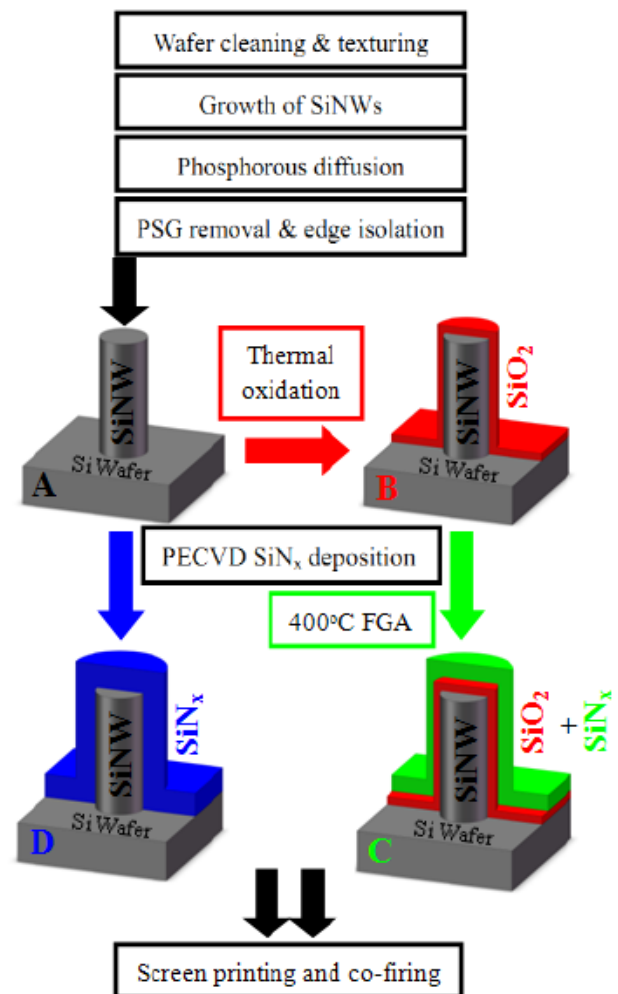

Figure 1. Schematic fabrication process diagrams of the SiNW based solar cells with different passivations for series A (in black, bare SiNWs without dielectric shell); B (in red, thermal oxidation of ~10 nm SiO$_2$ layer); C (in green, thermal oxidation ~10 nm SiO$_2$ layer combined with 60 nm SiN$_x$ deposition); and D (in blue, 70 nm SiN$_x$ deposition only).

passivation); series B (thermal oxidation at 850 °C for 20 min in N$_2$/O$_2$ ambient, i.e., ~10 nm SiO$_2$); series C (same thermal oxidation (~10 nm SiO$_2$) and another plasma-enhanced chemical vapor deposition (PECVD)-deposited 60 nm SiN$_x$ layer, then forming gas annealing (FGA) at 400 °C for 15 min); and series D (PECVD-deposited 70 nm SiN$_x$ layer). It should be noted that a ~10 nm SiO$_2$ layer is sufficient for the passivation of nanowires, since Schmidt *et al* [24] have demonstrated that the effectiveness of SiO$_2$ passivation is insensitive to its thickness in the range of 6–75 nm on silicon wafers, and Krylyuk *et al* [25] have reported that ~6 nm thickness of SiO$_2$ is sufficient for the Si nanowire device performance. Also, 60–70 nm SiN$_x$ layer thickness has been widely employed in the current mass production of Si solar cells with effective passivation and good anti-reflection. All the wafers went through the same Al back-surface-field formation, screen-printed front and back electrodes, and electrode metallization. Each series has three groups according to different etching times (100,
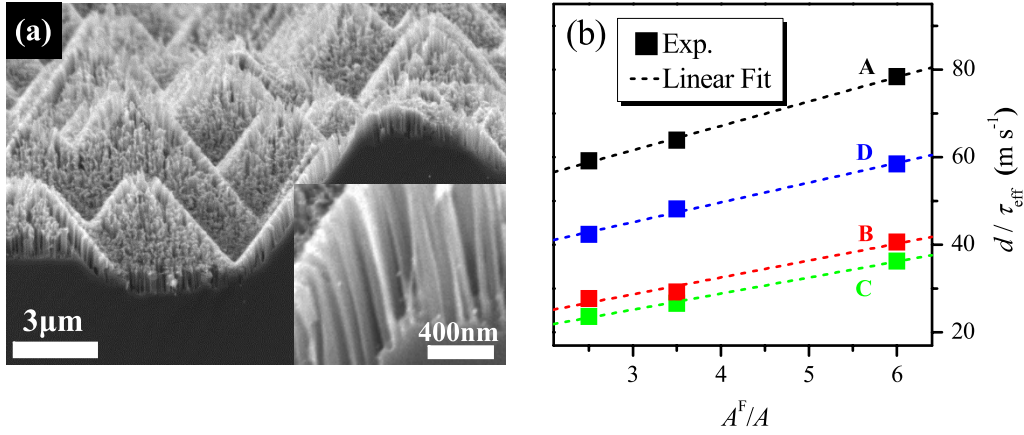
Figure 2. (a) SEM image (cross-sectional view) of initial SiNWs on textured silicon wafers etched for 400 s; the inset is the corresponding high magnification image. (b) Dependence of the measured d/τ_{eff} on the surface area enhancement ratio A^{F}/A for all series A–D, where the scatter points refer to experimental data and the lines denote the linear fit results.

200, and 400 s, corresponding to the length of SiNWs ∼300, ∼500, and ∼1000 nm, respectively), and each group has six wafers taking the statistic analysis into account. Each group is labeled by a combination of capital letter plus numeral, where the capital letter denotes the method of passivation and the numeral stands for the SiNW length in the unit of 100 nm. For example, B3 represents the thermal oxidation passivation with the SiNW length of 300 nm.

The morphologies of the SiNW based solar cells were examined by field emission scanning electron microscopy (FE-SEM, FEI Sirion 200). The minority carrier lifetime was taken by using the quasi-steady state photoconductance decay method (PV2000, Semilab). Both the optical reflectance and incident photon-to-current efficiency measurements, which were evaluated to characterize the external quantum efficiency of the samples, were made in the 300–1100 nm wavelength range by a PVE 300 photovoltaic device characterization system, Bentham Instruments. The current–voltage (*I–V*) characteristics of the SiNW based solar cells were measured at standard test conditions (an irradiation intensity of 1000 W m^{-2}, AM 1.5G, and a temperature of $24 \pm 0.5\,^{\circ}$C) using a solar simulator (Xenon lamp collector xec-1003s) and a sourcemeter (Keithley 3706A-NFP).

3. Passivation effect

Figure 2(a) presents the cross-sectional view of a typical surface morphology image of initial SiNWs on textured silicon wafers etched for 400 s, and the inset is the corresponding high magnification image. We can see that the length of the SiNWs is ∼1000 nm on the pyramid structure of planar silicon and the diameter of the SiNWs lies in the range of 60–200 nm, with an average diameter and period of about 100 nm and 250 nm, respectively. A simple geometric method has been employed to estimate the effect of surface area enhancement due to the SiNW growth. The front surface area of textured Si wafers (*A*) is about 1.73 times that of planar wafers, which is about 268 cm^2 for the 125 mm × 125 mm wafers. From the SEM observation, we have a total lateral area

of the SiNWs on textured wafers of about 1345 cm^2. The front surface area of the SiNW based wafers (A^{F}) includes both the total lateral area of the SiNWs and the pure textured Si wafer area *A*, which yields a surface area enhancement ratio A^{F}/A of 6.02. For different lengths of SiNWs, we have observed a length of 300 and 500 nm for the etching time of 100 and 200 s, which yields the surface area enhancement ratio of 2.50 and 3.51, respectively. In addition, the SiNWs are found to be along the silicon ⟨100⟩ crystallographic orientation, which is different from the previous result, where SiNWs were prepared in the vertical direction of the (1, 1, 1) facet of pyramid sidewalls [10]. This is due to the fact that the growth of SiNWs is a result of anisotropic etching of silicon by Ag nanoparticles [6, 26]. During the etching process, competition exists in different etching directions. At low temperature (in our case, room temperature), Ag nanoparticles prefer to move along the lowest energy ⟨100⟩ direction, while at high temperature (such as 50 °C) in [10], they would like to move along the ⟨111⟩ direction.

We have measured the effective minority carrier lifetime (τ_{eff}) in order to study the passivation effect on SiNW based wafers with different surface area enhancement ratios. In silicon with a diffused emitter, τ_{eff} of minority carriers could be expressed as [20]

$$\frac{1}{\tau_{\text{eff}}} = \frac{1}{\tau_{\text{bulk}}} + (S_{\text{eff}}^{\text{F}} + S_{\text{eff}}^{\text{B}})/d, \qquad (1)$$

where τ_{bulk} is the bulk Shockley–Read–Hall (SRH) lifetime, $S_{\text{eff}}^{\text{F}}$ and $S_{\text{eff}}^{\text{B}}$ are the effective surface recombination velocity at the front surface and at the back surface, respectively, and *d* is the wafer thickness (in our case, $d = 200\ \mu$m). Assuming that τ_{bulk} does not change during solar cell processing and the wafers have the same $S_{\text{eff}}^{\text{B}}$ for the same passivation method, we can transform equation (1) to

$$d/\tau_{\text{eff}} = S_{\text{loc}}^{\text{F}} A^{\text{F}}/A + (d/\tau_{\text{bulk}} + S_{\text{eff}}^{\text{B}}), \qquad (2)$$

on the basis that $S_{\text{eff}}^{\text{F}}$ scales up with the surface area for nanostructured front surfaces:

$$S_{\text{eff}}^{\text{F}} = S_{\text{loc}}^{\text{F}} A^{\text{F}}/A, \qquad (3)$$
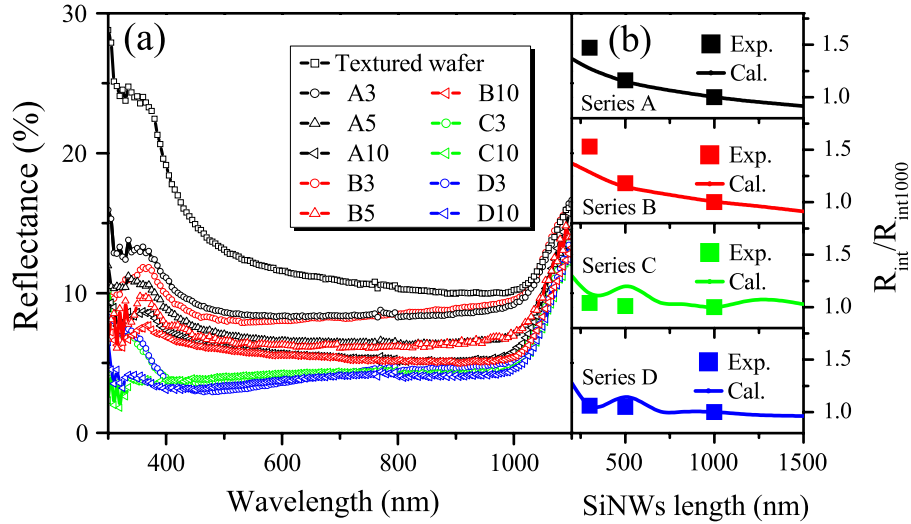
Figure 3. (a) Experimental reflectance spectra of the different groups of SiNWs on textured silicon wafers in the wavelength range of 300–1100 nm, together with the data of a textured wafer for comparison. (b) Experimental and FDTD calculated relative ratio of reflectance ($R_{int}/R_{int1000}$) versus the SiNW length for all series A–D. R_{int} is the integrated reflectance obtained by weighting over the AM 1.5G solar spectrum in the range 300–1100 nm while $R_{int1000}$ is the integrated reflectance at an SiNW length of 1000 nm.

where S_{loc}^{F} is the local effective surface recombination velocity at and very near the actual front surface. We can further assume the whole SiNW region as n type after diffusion with the same doping concentration distribution, i.e., S_{loc}^{F} is independent of the length of SiNWs. This assumption has actually been validated by the transient photoconductance decay method [20], where S_{eff}^{F} (determined from the measured τ_{eff}) is found to be linear with the surface area enhancement ratio A^{F}/A in nanostructured silicon wafers with n^{+}–p junctions.

As a result of (2), the measured d/τ_{eff} is expected to also be linear with A^{F}/A. This is actually what we have observed in figure 2(b), where the slope of each curve is equivalent to S_{loc}^{F} of each passivation. Different passivation treatments will yield different S_{eff}^{F}, and therefore different S_{loc}^{F}. The values of S_{loc}^{F} for the four different kinds of passivation series A, B, C, and D are found to be 5.56, 3.85, 3.66, and 4.51 m s^{-1}, respectively, demonstrating that the SiO$_2$/SiN$_x$ stack (series C) exhibits the best passivation effect with a good suppression to the surface recombination of SiNWs. Compared to the single layer of SiO$_2$, the SiO$_2$/SiN$_x$ stack structure contains hydrogen in SiN$_x$ and could realize hydrogen passivation, which effectively reduces the SRH recombination (see section 5). On the other hand, the SiO$_2$ layer is grown by thermal oxidation, which would form a homogeneous layer around the nanowire to reduce the surface recombination [25]. Therefore, the SiO$_2$/SiN$_x$ stack structure has lower surface recombination velocity than a single layer of SiO$_2$ or SiN$_x$.

4. Reflectance characteristics

We have also examined the influence of different dielectric surface passivations on the optical properties of SiNW based wafers. In figure 3(a), we show the reflectance spectrum of each group over the wavelength range of 300–1100 nm, and

the data of a textured wafer is also given for comparison. Clearly, suppressed reflection over entire spectral range is obtained for all series compared to the only textured wafer, which surely indicates the great improvement of SiNWs in anti-reflection performance. Also, we can observe that in each series longer SiNWs have lower reflection than shorter samples. This NW-length-dependent behavior of reflection is mainly attributed to the prolonged optical path length in structure, matching well with the work in the literature [10]. Besides, groups with different passivations show varied effects. Comparing series B to series A, we can see that the presented spectra of A3 and B3, A5 and B5, A10 and B10 are quite similar over a broad range of wavelength, demonstrating little benefit for anti-reflection from the thermal oxidation process. On the other hand, SiNWs with SiN$_x$ layers (groups C3, C10, D3, and D10) possess almost identical and very low reflectance (~4.6%) despite the change of SiNW length and passivation method. This can be explained in that the SiN$_x$ passivation layer provides such good anti-reflection characteristics that it even dominates over the length-dependent light trapping effect of SiNWs.

We further simulate the anti-reflection performance of the different dielectric surface passivations with the FDTD calculation. SiNWs with varied lengths of 200–1500 nm are modeled on a flat substrate, with different dielectric layers corresponding to the four series A–D. Both experimental and theoretical integrated reflectance (R_{int}) are obtained by weighting over the AM 1.5G solar spectrum in the range of 300–1100 nm. Note that since our simulation is carried out on a flat substrate, which agrees well with other researchers [14], we utilize a relative ratio $R_{int}/R_{int1000}$, i.e. the ratio of integrated reflectance R_{int} to the value at SiNW length 1000 nm, to help eliminate the impact of the textured substrate. We can see that the calculated results are to some extent consistent with the experimental observation, as shown in figure 3(b). For series A and B, similar trends are observed,

which proves the small effect of ∼10 nm SiO$_2$ thermal oxidation layer as discussed above. The reflectance of SiNWs with short length below 1000 nm depends sensitively on NW length, while when the NW length grows higher than 1000 nm little improvement is achieved. As a result, we can conclude that under thin dielectric passivation (∼10 nm SiO$_2$ thermal oxidation) reflectance decreases slightly (∼0.2%) and the length-dependent light trapping effect of SiNWs plays the dominant role. By contrast, when we turn to series C and D, it is found that quite low reflectance can be obtained even at the very short length of 300 nm, and remains nearly unchanged with increasing SiNW length. The fluctuation of theoretical results between 300 and 500 nm is due to the merged Mie scatting resonances for thick dielectric layers in perfect subwavelength structures such as NWs [27]. Actually, in a practical experiment the SiNWs could not be perfectly arranged especially at the bottom, thus disturbing the structure turns out to have a positive effect in getting stable low reflectance (∼4.6%). Therefore, it is clear that the anti-reflection of thick dielectric passivation layers (series C and D) becomes significant as the key role, even making the length-dependent light trapping of SiNWs negligible. Subsequently, the passivation by a thick dielectric layer (series C and D) not only efficiently suppresses the surface recombination (see section 5), but also serves as a prominent way to obtain excellent anti-reflection performance simultaneously, even at very short SiNW length.

5. Carrier recombination

We now focus on the charge collection efficiency of photons absorbed at and near SiNWs for better understanding the carrier recombination processes, and therefore to suppress the carrier recombination for high efficiency SiNW based solar cells. The internal quantum efficiency (IQE) of these SiNW based solar cells has been derived from the external quantum efficiency (EQE) characteristics via IQE = EQE/(1 − R), where the EQE has been characterized from the incident photon-to-current efficiency measurement in the wavelength range of 300–1100 nm and R is the reflectance presented in figure 3(a). Figure 4(a) shows the averaged IQE spectra from the cells of A3, B3, C3, and D3 (each group cell has six samples). The group A3 cell (bare SiNWs without any passivation) exhibits a very low value of IQE, which has been explained by large surface recombination and high Auger recombination [20]. The photogenerated carriers have little chance of being collected at the cell surface, leading to the observed poor blue spectral response. The high Auger recombination further significantly degrades the IQE at the wavelengths from 600 to 950 nm due to the absorption of longer wavelength photons in the excessive doping of the SiNWs after the diffusion process. In contrast, we can easily see in figure 4(a) that the IQE data of the cells with passivation treatment (groups B3, C3, and D3) have been greatly improved; in particular, the group C3 cell (∼10 nm SiO$_2$ + 60 nm SiN$_x$) gives the best result. As discussed in the passivation part of section 3, the surface recombination velocity has been reduced after the passivation treatment and
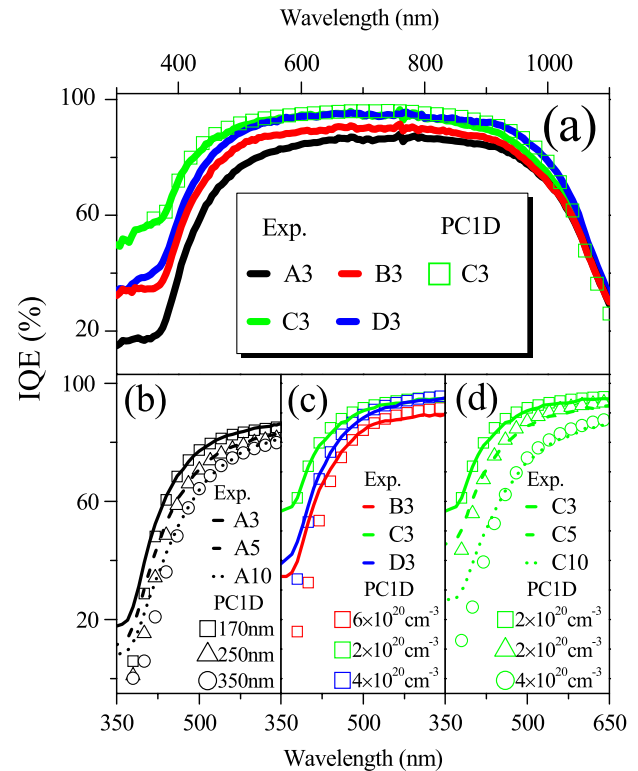

Figure 4. (a) Experimental averaged IQE spectra of the group cells of A3, B3, C3, and D3 in the wavelength range of 300–1100 nm, together with the calculated IQE spectrum of C3 (scatter points) from the PC1D simulation based on 'the dead layer' model. (b)–(d) Experimental averaged IQE spectra (curves) and the calculated IQE results from the PC1D simulations (scatter points) of different group cells in the short wavelength range of 350–650 nm.

the SiO$_2$/SiN$_x$ stack (series C) exhibits the best passivation effect; the improved IQE could be attributed to the lower SRH and Auger recombination.

The IQE in the short wavelength region relates to the recombination near the front surface. In the series A cells with very large surface recombination and high Auger recombination, we can treat the SiNWs as a low lifetime 'dead layer' and model the IQE (figure 4(b)) by implementing the SiNW 'dead layer' as a heavily doped n-type Si (∼1 × 10^{21} cm^{-3}) [9] using the one-dimensional device program PC1D. It is shown in figure 4(b) that the 'dead layer' thickness in the group A3 cell is about 170 nm, while the calculation (scatter points) for the group A5 and A10 cells gives the thicknesses of 250 and 350 nm, respectively. This indicates that the surface and Auger recombination in the bare SiNWs without any passivation rise with the surface area enhancement during the diffusion process. SiNWs worsen both the surface state channel (via increasing the surface area) and the Auger recombination channel (via altering the doping profile). Yuan *et al* [9] have observed similar behavior between the thickness of the nanoporous 'dead layer' and the growth time of 'black silicon'.

In heavily doped silicon, dislocation and dangling bonds are generated due to the mismatch between the covalent radius of an impurity atom that is occupying a substitutional site and that of silicon, which could lead to severe SRH

recombination [28]. Therefore, the recombination in the low lifetime 'dead layer' is not only Auger recombination, but also the SRH recombination (or the doping density in a way represents recombination rate per volume). We have demonstrated in figure 4(c) the effect of different passivation techniques on the carrier recombination of the SiNW based solar cells (groups B3, C3, and D3 with the same SiNW length of 300 nm, i.e. the same surface area enhancement ratio of 2.50). In the 'dead layer' model, we maintain the 'dead layer' thickness of ∼170 nm for the case of 300 nm SiNW length but change the doping density. It is shown that after passivation the doping density of groups B3, C3, and D3 reduces to 6×10^{20}, 2×10^{20}, and 4×10^{20} cm^{-3}, respectively, illustrating that all the applied passivation techniques decrease the recombination rate per volume in the 'dead layer'.

For the origin of the reduced doping density, it is reported that the thermal oxidation process would modify the surface concentration and lead to a lower surface doping density [29], while the bulk SRH recombination is still high in the thin (∼10 nm) SiO_2 passivation cells (series B). Therefore, the decreased surface recombination in the group B3 cells can be attributed to the reduced doping density. On the other hand, hydrogen is contained in SiN_x layers because we use silane (SiH_4) and ammonia (NH_3) gases as the sources in PECVD to deposit the thick (70 nm) SiN_x layers. During the firing process, hydrogen would be released and passivate the dislocations and dangling bonds. SiN_x can act as not only surface passivation but also bulk passivation due to the hydrogen diffusion. Auger recombination can also be weakened to some extent since it is related to the numbers of defect states [22]. As a result, the lower SRH and Auger recombination is due to the reduced doping density in the group D3 cell. The group C3 cell shows the lowest doping density, which results from the combined effect of the thermal oxidation and the hydrogen passivation. In a word, the SiO_2/SiN_x stack exhibits the best passivation effect on heavily doped SiNWs through reducing both the SRH recombination and Auger recombination.

We can further show in figure 4(d) the different passivation mechanisms in the SiO_2/SiN_x stacks (series C cells) with different lengths of heavily doped SiNWs. As observed in figure 4(b), the 'dead layer' thickness increases with the SiNW length, an indication of enhancing both the SRH and Auger recombination there. Here we have also employed the 'dead layer' thicknesses of about 170, 250, and 350 nm for the three samples C3, C5, and C10, respectively. Since all three samples go through the same thermal oxidation process, the reduced surface recombination would be the same. Less effective SiO_2/SiN_x stack passivation in the group C10 cell with a doping density of 4×10^{20} cm^{-3} could be ascribed to the limited hydrogen in the SiN_x layer, which only passivates fixed SRH recombination. In short, heavily doped SiNWs contain severe Auger and SRH recombination processes. Thermal oxidation would reduce the surface recombination while hydrogen would effectively passivate the SRH recombination channel. The observed better performance of series C and D than that of series A and B is mainly due to the hydrogen passivation, rather than the
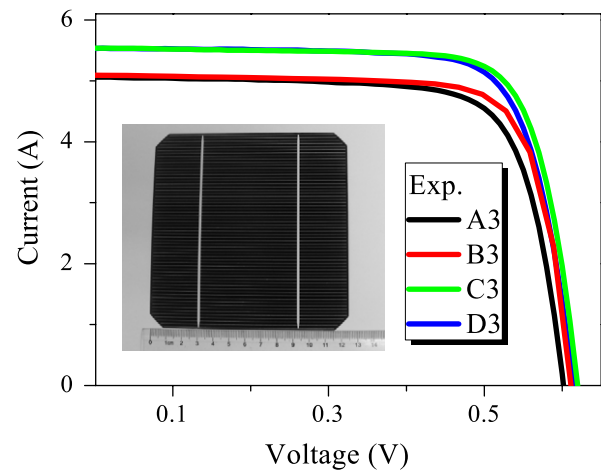

Figure 5. Current–voltage characteristics of the group cells of A3, B3, C3, and D3 under AM 1.5G illumination, together with the image of the group C3 cell (conversion efficiency of 17.11% and area of 125×125 mm^2) shown in the inset.

passivation layer thickness difference. A satisfied hydrogen passivation effect has been achieved on the group C3 and C5 cells with short heavily doped SiNWs.

6. Cell performance

Finally, we show the output performance of our cells to evaluate the comprehensive impact of the passivation discussed above. Figure 5 demonstrates the *I–V* curves of our best cells in each series (i.e., groups A3, B3, C3, and D3). Clearly, the group C3 cell achieves the best output performance among the four SiNW based solar cells with the open circuit voltage (V_{oc}) of 0.620 V, short circuit current (I_{sc}) of 5.536 A, fill factor (FF) of 77.20%, and efficiency (EFF) of 17.11%, while the group A3 cell exhibits the worst. This superiority of the group C3 cell benefits from the most effective surface and hydrogen passivation, as well as the best optical anti-reflection, which can be seen from the black front surface as shown in the inset of figure 5. Our result (17.11%) is now a record for a nanostructure based Si solar cell with the large area of 125×125 mm^2 (154.83 cm^2), while an 18.2% efficient nanostructured Si solar cell has been achieved in the small size of 0.8081 cm^2 very recently [20].

For detailed comparison, we illustrate the electrical parameters for each group in table 1 (all values are obtained as averages over each group's six samples). The reverse saturation current (I_0) and diode quality factor (n), which are extracted from the illuminated *I–V* measurements [30], can relatively represent the passivation effect because of its correspondence to the total recombination including both the Auger and SRH recombination in a solar cell [31]. We notice that in each series longer SiNW based solar cells show larger values of I_0 and n than shorter samples, indicating increases of both the Auger and SRH recombination in the n-type region. Compared to series A, the values of I_0 and n of series B, C, and D with the same length decrease after passivation, revealing

Table 1. Averaged electrical parameters, i.e., the open circuit voltage (V_{oc}), short circuit current (I_{sc}), fill factor (FF), efficiency (EFF), extracted reverse saturation current (I_0), and extracted diode quality factor (n) of different groups of SiNW based solar cells, as well as the integrated reflectance R_{int} by weighting the reflectance in figure 3(a) over the AM 1.5G solar spectrum in the range 300–1100 nm. Series A–D represents the SiNW based solar cells without passivation and passivated by ~10 nm SiO_2, by ~10 nm SiO_2 + 60 nm SiN_x, and by 70 nm SiN_x, respectively. The numeral stands for the SiNW length in the unit of 100 nm, e.g., B3 represents the thermal oxidation passivation with the SiNW length of 300 nm.

	V_{oc} (V)	I_{sc} (A)	FF (%)	EFF (%)	I_0 (A)	n	R_{int} (%)
A3	0.599	5.055	73.76	14.41	9.678×10^{-7}	1.42	9.150
A5	0.598	5.011	72.95	14.11	2.581×10^{-6}	1.58	7.238
A10	0.571	4.869	62.51	11.23	1.930×10^{-4}	1.94	6.232
B3	0.611	5.133	76.47	15.38	7.212×10^{-8}	1.29	9.005
B5	0.606	5.118	75.07	15.00	7.767×10^{-7}	1.44	6.956
B10	0.592	4.913	72.08	13.54	6.594×10^{-6}	1.58	5.904
C3	0.619	5.532	76.68	16.96	2.384×10^{-8}	1.21	4.812
C5	0.613	5.410	76.20	16.33	5.621×10^{-8}	1.26	4.638
C10	0.594	5.047	71.41	13.82	1.153×10^{-6}	1.47	4.608
D3	0.614	5.516	76.00	16.64	3.762×10^{-8}	1.22	4.634
D5	0.608	5.372	75.74	16.12	1.205×10^{-7}	1.33	4.562
D10	0.590	5.027	69.50	13.44	2.507×10^{-6}	1.52	4.351

the suppression of the SRH recombination. Moreover, the group C3 cell shows the smallest I_0 and n, implying the lowest Auger and SRH recombination in the n-type region. All these results agree well with our discussion in sections 3 and 5 about the passivation effect and carrier recombination.

We further turn to understand the relationship between the short circuit current I_{sc} and the integrated reflectance R_{int} of each group (see table 1). It is found that close values of R_{int} (e.g., the R_{int} of groups A3 and B3 is 9.150, 9.005%, respectively) lead to a very near result of I_{sc} (e.g., the I_{sc} of groups A3 and B3 is 5.055, 5.133 A, respectively) for groups with same SiNW lengths. This is attributed to the dominating role of R_{int} over I_{sc} at fixed SiNW length. On the other hand, the changed R_{int} for the group C3 cell (4.812%) compared with the group A3 cell (9.150%), obtained by using the SiO_2/SiN_x stack, results in an observed increment of 0.477 A in I_{sc}, which is actually due to the combined effect of the surface passivation and R_{int} reduction. However, when it comes to the group A5 cell, the dropped R_{int} compared to that of the A3 cell, obtained by increasing the length of SiNWs (i.e. an increase in the surface enhancement ratio from 2.50 to 3.51), leads to a small reduction of 0.044 A in I_{sc}, which could be ascribed to the balanced effect between the surface/Auger recombination enhancement and R_{int} reduction. Besides, due to the effective surface passivation of the SiO_2 layer, the group B5 cell (similar R_{int} to that of the group A5 cell) exhibits even larger I_{sc} than that of the group A3 cell. These results demonstrate that different R_{int} reducing approaches by deposition of a dielectric layer or by increasing SiNW length will have different effects on I_{sc}, and application of even a thin dielectric layer is better than bare SiNW length increase due to its anti-reflection effect and surface passivation effect.

Nevertheless, the output performance of our best SiNW based solar cells (the group C3 cell with an efficiency of 17.11%) still needs improvement in various aspects. It is to some extent limited by the low IQE response in the whole wavelength associated with the Auger recombination as seen

in figure 4(a) and a poor optimized front electrical contact. Additionally, since we put two textured wafers together to make SiNWs only on one side, the edge region of the backside is inevitably etched with SiNWs, which will increase the back surface recombination and thus degrade the cell output performance. For further EFF increase, a carefully designed diffusion process is suggested, in order to minimize the unfavorable Auger recombination near the surface. A simple way is to design the cell with light and shallow doping and simultaneously controlling the surface recombination. The sheet resistance of our samples after diffusion is around 75 Ω/sq, while that of the 18.2% efficiency small cell is around 129 Ω/sq [20]. Besides, front electrical contact could be improved by selective growth of SiNWs in the active area or by a double-step diffusion process [11, 13] and the backside of the textured wafer could be protected by application of a photoresist during the etching process. Furthermore, more detailed study on the SiO_2/SiN_x stack passivation, such as growth temperature, source gas ratio, posthydrogen process, etc, should be implemented to further decrease the recombination rate.

7. Conclusions

We have demonstrated an effective and industrially compatible technique of dielectric passivation to improve the electrical properties of SiNW based solar cells while maintaining the excellent optical properties of SiNW structure. SiN_x passivation exhibits good reduction of defect state density and suppression of the Auger recombination due to the well known surface passivation and hydrogen-diffusion-induced bulk passivation. We have further combined with the SiO_2 surface passivation to obtain the best SRH and Auger recombination suppression both at and near the SiNW surface. Through detailed investigation of the effects of different passivations and SiNW lengths on the effective minority carrier lifetime, reflectance and carrier recombination characteristics, as well as cell performance, we have successfully achieved

the highest record conversion efficiency of 17.11% for SiNW based solar cells with a SiO_2/SiN_x stack passivation on a large area of 125×125 mm^2. Since both the growth of SiNWs and the dielectric passivation can be carried out in the present industrial manufacturing processes, this work opens a potential prospect for the mass production of high efficiency SiNW based solar cells with small modifications of the diffusion process and the SiO_2/SiN_x stack passivation.

Acknowledgments

References

[1] Hu L and Chen G 2007 Analysis of optical absorption in silicon nanowire arrays for photovoltaic applications *Nano Lett.* **7** 3249–52

[2] Tsakalakos L *et al* 2007 Strong broadband optical absorption in silicon nanowire films *J. Nanophoton.* **1** 013552

[3] Srivastava S K, Kumar D, Singh P K, Kar M, Kumar V and Husain M 2010 Excellent antireflection properties of vertical silicon nanowire arrays *Sol. Energy Mater. Sol. Cells* **94** 1506–11

[4] Kayes B M, Atwater H A and Lewis N S 2005 Comparison of the device physics principles of planar and radial p–n junction nanorod solar cells *J. Appl. Phys.* **97** 114302

[5] Peng K Q, Xu Y, Wu Y, Yan Y J, Lee S T and Zhu J 2005 Aligned single-crystalline Si nanowire arrays for photovoltaic applications *Small* **1** 1062–7

[6] Fang H, Li X D, Song S, Xu Y and Zhu J 2008 Fabrication of slantingly-aligned silicon nanowire arrays for solar cell application *Nanotechnology* **19** 255703

[7] Perraud S, Poncet S, Noel S, Levis M, Faucherand P, Rouviere E, Thony P, Jaussaud C and Delsol R 2009 Full process for integrating silicon nanowire arrays into solar cells *Sol. Energy Mater. Sol. Cells* **93** 1568–71

[8] Shu Q K *et al* 2009 Hybrid heterojunction and photoelectrochemistry solar cell based on silicon nanowires and double-walled carbon nanotubes *Nano Lett.* **9** 4338–42

[9] Yuan H C, Yost V E, Page M R, Stradins P, Meier D L and Branz H M 2009 Efficient black silicon solar cell with a density-graded nanoporous surface: optical properties, performance limitations, and design rules *Appl. Phys. Lett.* **95** 123501

[10] Chen C *et al* 2010 Silicon nanowire-array-textured solar cells for photovoltaic application *J. Appl. Phys.* **108** 094318

[11] Chen C, Jia R, Li H F, Meng Y L and Liu X Y 2011 Electrode-contact enhancement in silicon nanowire-array-textured solar cells *Appl. Phys. Lett.* **98** 143108

[12] Toor F, Branz H M, Page M R, Jones K M and Yuan H C 2011 Multi-scale surface texture to improve blue response of nanoporous black silicon solar cells *Appl. Phys. Lett.* **99** 103501

[13] Kumar D, Srivastava S K, Singh P K, Husain M and Kumar V 2011 Fabrication of silicon nanowire arrays based solar

cell with improved performance *Sol. Energy Mater. Sol. Cells* **95** 215–8

[14] Huang B R, Yang Y K, Lin T C and Yang W L 2012 A simple and low-cost technique for silicon nanowire arrays based solar cells *Sol. Energy Mater. Sol. Cells* **98** 357–62

[15] Jia G B, Steglich M, Sill I and Falk F 2012 Core–shell heterojunction solar cells on silicon nanowire arrays *Sol. Energy Mater. Sol. Cells* **96** 226–30

[16] Liu Y P *et al* 2012 Nanostructure formation and passivation of large-area black silicon for solar cell applications *Small* **8** 1392–7

[17] Wang X, Peng K Q, Pan X J, Chen X, Yang Y, Li L, Meng X M, Zhang W J and Lee S T 2011 High-performance silicon nanowire array photoelectrochemical solar cells through surface passivation and modification *Angew. Chem. Int. Edn* **50** 9861–5

[18] Kim J Y, Kwon M K, VJ L, Grego S and Islam M S 2012 Postgrowth *in situ* chlorine passivation for suppressing surface-dominant transport in silicon nanowire devices *IEEE Trans. Nanotechnol.* **11** 782–7

[19] Zhao J H, Wang A H and Green M A 1999 24.5% efficient silicon PERT cells on MCZ substrates and 24.7% efficiency PERL cells on FZ substrates *Prog. Photovolt., Res. Appl.* **7** 471–4

[20] Oh J, Yuan H C and Branz H M 2012 An 18.2%-efficiency black-silicon solar cell achieved through control of carrier recombination in nanostructures *Nature Nanotechnol.* **7** 743–8

[21] Aberle A G 2000 Surface passivation of crystalline silicon solar cells: a review *Prog. Photovolt., Res. Appl.* **8** 473–87

[22] Kerr M J and Cuevas A 2002 General parameterization of Auger recombination in crystalline silicon *J. Appl. Phys.* **91** 2473–80

[23] Xie W Q, Oh J I and Shen W Z 2011 Realization of effective light trapping and omnidirectional antireflection in smooth surface silicon nanowire arrays *Nanotechnology* **22** 065704

[24] Schmidt J, Kerr M and Cuevas A 2001 Surface passivation of silicon solar cells using plasma-enhanced chemical-vapour-deposited SiN films and thin thermal SiO$_2$/plasma SiN stacks *Semicond. Sci. Technol.* **16** 164–70

[25] Krylyuk S, Davydov A V, Levin I, Motayed A and Vaudin M D 2009 Rapid thermal oxidation of silicon nanowires *Appl. Phys. Lett.* **94** 063113

[26] Chen C Y, Wu C S, Chou C J and Yen T J 2008 Morphological control of single-crystalline silicon nanowire arrays near room temperature *Adv. Mater.* **20** 3811–5

[27] Spinelli P, Verschuuren M A and Polman A 2012 Broadband omnidirectional antireflection coating based on subwavelength surface Mie resonators *Nature Commun.* **3** 692

[28] Yukimoto Y 1969 Defects induced by deep diffusion of phosphorus into silicon *Japan. J. Appl. Phys.* **8** 568–81

[29] Rohatgi A, Doshi P, Moschner J, Lauinger T, Aberle A G and Ruby D S 2000 Comprehensive study of rapid, low-cost silicon surface passivation technologies *IEEE Trans. Electron Devices* **47** 987–93

[30] Tivanov M, Patryn A, Drozdov N, Fedotov A and Mazanik A 2005 Determination of solar cell parameters from its current–voltage and spectral characteristics *Sol. Energy Mater. Sol. Cells* **87** 457–65

[31] Gray J L 2003 *Handbook of Photovoltaic Science and Engineering* ed A Luque and S Hegedus (New York: Wiley) chapter 3